DNA on Fluid Membranes: A Model Polymer in Two Dimensions

Berenike Maier and Joachim O. Rädler*

Institut für Biophysik (E22), Physik Department, Technische Universität München, James Franck Strasse 1, D-85747 Garching, Germany

Received January 18, 2000; Revised Manuscript Received May 31, 2000

ABSTRACT: The polymeric properties of DNA molecules, which are electrostatically bound to glass-supported cationic lipid membranes, are investigated. The electrostatic interaction is sufficiently strong to hold DNA flat onto the fluid lipid surface but allows DNA to diffuse freely in-plane. The molecules are fluorescently labeled, and fluorescence images are examined in terms of real-space monomer distributions of polymer chains. The chain extension of single DNA fragments of restriction enzyme digests shows power law scaling with number of base pairs in accordance with self-avoiding walks in two dimensions. Dynamic scaling is found for center-of-mass diffusion following Rouse dynamics, $D \sim 1/N$, and for rotational relaxation times, $\tau_r \propto N^{\mu}$ with $\mu = 2.6 \pm 0.4$. A crowded surface of monodisperse λ-DNA behaves like a two-dimensional semidilute solution with a measurable correlation length ξ being smaller than for dilute preparations. Polymer unbinding and the role of surface defects are discussed.

Introduction

In recent years direct imaging of single biological macromolecules shed new light on basic polymer science. Fluorescence labeling of DNA, actin, or microtubules made molecules directly observable as polymer chains in aqueous solution using optical light microscopy.[1] In particular, the size of biomolecules ranging from a few nanometers to almost millimeters allows direct quantitative analysis of various polymer properties as a power of polymer length. Polymer properties such as scaling laws predicted for flexible polymers have been directly measured as for example the chain self-diffusion,[2,3] hydrodynamic drag,[4,5] reptation motion in polymer gels,[6,7] or electrophoretic drift.[8,9] Furthermore, conformational changes, e.g., condensation upon complexation with cationic agents, are directly observable.[10,11] Most of these fluorescence studies are carried out in bulk solution. In this case Brownian motion limits the period of time that a single molecule is observable in the focal plane during experiments. For this reason optical tweezers are used to hold latex particles, which are chemically linked to DNA. The latex particles are handles, which allow to maneuver single biomolecules by means of optical forces. An alternative route to avoid out-of-focus drift is to restrict molecules to a flat surface. Unfortunately, bound molecules might lose much of their native bulk properties due to either steric hindrance or denaturation at the solid surface. However, many experimental imaging techniques require operation on solid substrates. Hence, the preparation of macromolecules on suitable adsorbing interfaces that allow to follow dynamical features is of general interest.

In a recent paper we have introduced cationic supported lipid membranes as fluid binding surfaces.[12] Cationic lipid membranes were fused on glass substrates, and DNA molecules adsorbed to them diffuse freely in plane as depicted in Figure 1. It was shown that in this situation chain extensions are in agreement with the theoretical scaling laws for self-avoiding chains.[12] In two dimensions exact analytic results[13] as well as Monte Carlo studies[14,15] exist. However, experimental studies on polymers in two dimensions are very limited. Hence, in this article we like to focus on DNA bound to supported membranes as a model system for 2D polymer physics. First, we review in detail the preparation and analysis of quasi-two-dimensional DNA molecules. The static and dynamic scaling of single molecules is analyzed. In particular, the rotational relaxation is examined here for the first time in two dimensions. Solutions of monodisperse λ-DNA are in-

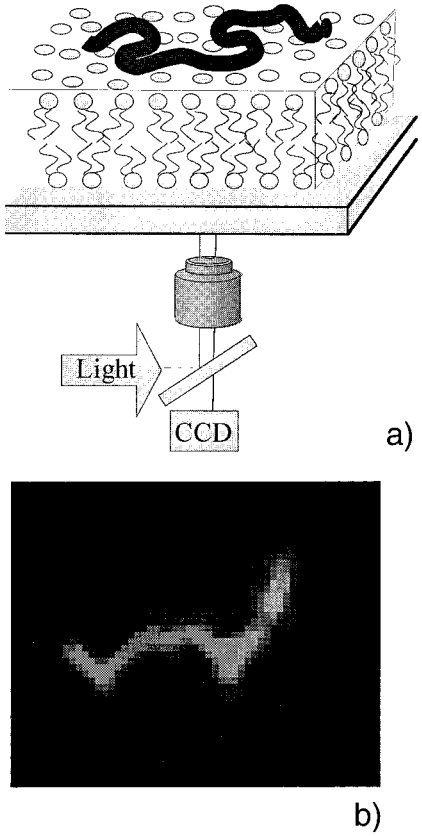

Figure 1. (a) Schematic drawing of the experimental setup: DNA adsorbed to a cationic supported lipid bilayer is visualized by fluorescence microscopy. (b) Typical image of an isolated λ-DNA molecule. The fluorescence intensity distribution is proportional to the polymer monomer density (bar = 10 μm).

* Corresponding author. E-mail: raedler@ph.tum.de.

10.1021/ma000075n CCC: $19.00
Published on Web 08/23/2000

vestigated and proved to behave like two-dimensional semidilute polymer solutions. Furthermore, the unbinding of the semiflexible DNA polyelectrolyte chains with increasing bulk salt concentration is studied. Finally, the role of surface defects on the adsorbed molecules is demonstrated.

Experimental Section

Materials and Preparation. Substrate-supported membranes were prepared by vesicle fusion using sonicated vesicles. If not mentioned differently, microscopy cover glass was used as solid substrate. Cover slides were cleaned in 2% Hellmanex solution (Hellma, Germany), rinsed, and dried thoroughly and subsequently mounted onto a Teflon frame. The sonicated cationic vesicles were prepared as follows: dioleoyltrimethylammonium−propane (DOTAP) and dioleoyl-1,2-*sn*-phophatidylcholine (DOPC) (Avanti Polar Probes, Birmingham, AL) were mixed at a mass ratio 1:10 in chloroform. The mixed lipid chloroform solutions were dried overnight in a vacuum chamber, resuspended in bidistilled water (Millipore, Eschborn) for 1 h at 40 °C, and sonicated for 10 min in a tip sonicator (Branson). The vesicle solution was filled into the measuring chamber with freshly cleaned glass surfaces and incubated for 10 h. After this period of time the chamber was carefully rinsed with buffer solution. Supported lipid bilayers formed by this method were inspected by fluorescence microscopy using 0.02% Texas-Red-DHPE lipid and found to be entirely homogeneous and fluid.

λ-phage DNA was purchased from Boehringer Mannheim and cut using the restriction enzymes ApaI, BbrPI, SacI, and XbaI according to the manufacturer's procedure. The length distribution was checked by gel electrophoresis. After labeling with the intercalating dye TOTO (Molecular Probes) at a dye/bp ratio 1/5, DNA was adsorbed to the supported membrane in 10 mM HEPES buffer. After 10 min incubation excess DNA was removed by rinsing with the working buffer (10 mM HEPES, pH 7, 10 mM NaCl, if not noted otherwise).

The experiments described in the following are extremely sensitive to the quality of the underlying lipid bilayer and buffer conditions. For example, standard reagents used to avoid photodamage were found to exhibit adverse effects on the DNA conformations. Mercaptoethanol induces DNA collapse on the lipid surface; glucose oxidase in combination with catalase immobilizes the DNA. To date, the only antioxigent found without measurable effect on DNA conformation or mobility was ascorbic acid (0.5 mM) as used by us in particular for the semidilute preparations. Furthermore, it is crucial to allow the sample to relax. Experiments were not started earlier than 1 h after sample preparation. Semidilute preparations were equilibrated for more than 1 day to ensure thermodynamic equilibrium. Ionic strengths of 10−30 mM NaCl are optimal for efficient equilibration. All experiments were performed at room temperature.

Fluorescence Microscopy and Image Acquisition. An inverted Zeiss Axiovert 135TV microscope equipped with fluorescence filter sets, and a 100× (NA1.3) or 63× (NA1.25) oil immersed objective was used for the single molecule observations. DNA-TOTO and Texas-Red-DHPE were excited with a shutter-controlled high-pressure mercury lamb at 450−490 and 530−585 nm, respectively. Fluorescence emission was detected at 520 or 615 nm by means of a cooled digital 12-bit CCD camera (Princeton Instruments) at a typical rate of 3 frames/s. The data collection and image processing was carried out by the image analysis system IPLab (Scanalytics).

Analysis of Single Molecule Fluorescence. After subtraction of the background a threshold was set in order to divide the image into subframes encompassing a single DNA molecule. The intensity distribution $I(r,t)$ of each subframe was analyzed by standard IPLab tools. The zeroth moment accounts for the total fluorescence intensity of one DNA molecule.

$$I(t) = \int I(\mathbf{r},t)\, \mathrm{d}\mathbf{r} \tag{1}$$

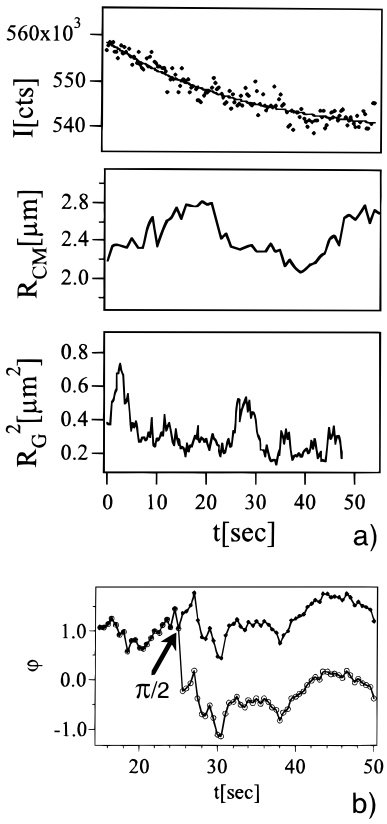

Figure 2. (a) Typical raw data showing evolution of the zeroth, first, and second moment of the intensity distribution of a single DNA molecule over time. (b) Time course of the direction of the longer principal axis of the radius of gyration tensor. The arrow indicates an incident when the principal axes jumps after passing through a circular shape.

Assuming the fluorescent label is homogeneously distributed within a DNA molecule, the total fluorescence intensity is proportional to the length of the DNA segment. The first moment of the intensity distribution denotes the position of the center of mass

$$\mathbf{R}_{\mathrm{cm}}(t) = \frac{1}{I(t)} \int \mathbf{r} I(\mathbf{r},t)\, \mathrm{d}\mathbf{r} \tag{2}$$

The second moment is the gyration tensor of the intensity distribution.

$$M_{ij}(t) = \frac{1}{I(t)} \int (r_i - R_{\mathrm{cm},i})(r_j - R_{\mathrm{cm},j}) I(\mathbf{r},t)\, \mathrm{d}\mathbf{r} \tag{3}$$

which yields by definition the common radius of gyration

$$R_{\mathrm{G}}^2 = \mathrm{trace}(M_{ij}) \tag{4}$$

An example of a short time sequence of the zeroth, first, and second moment of the fluorescence intensities is shown in Figure 2. The zeroth moment, which gives the total fluorescence, shows little fluctuations, but a systematic slow exponential decrease over time due to photobleaching. The second graph represents the x-coordinate of the center-of-mass vector of the molecule. Clearly random translational motion is observed, which we will deal with in detail in one of the following paragraphs.

Since the second moment of the fluorescence distribution is a tensor,[16] DNA is described as an ellipse with its longer principal axis oriented at angle

$$\varphi(t) = \mathrm{arctg}\left(\frac{\lambda(t) - M_{xx}(t)}{M_{xy}(t)}\right) \tag{5}$$

where $\lambda(t)$ is the eigenvalue of the longer axis. In general, the orientational variation between two successive frames $\Delta\varphi = \varphi_{i+1} - \varphi_i$ is small; $\Delta\varphi \ll \pi/2$. Occasionaly, however, especially for short fragments, discontinuities occur, as shown in Figure 2b. They are interpreted as follows: If molecules pass through a circular shape, the directional memory is lost. In this case the calculated angle φ jumps. For each frame we calculated the unit vector $\mathbf{u}_{n+1}$ for each quadrant and chose the smallest jump angle. However, not more than three jumps were observed in a sequence of 150 images, and thus the effect of these discontinuities is negligible on the time scale relevant for our experiments.

Fourier Transformation of DNA Ensemble Images. The structure factor of dilute and semidilute images of adsorbed DNA was determined by Fourier transformation. After background correction a 1024 × 1024 or 512 × 512 image was transformed by standard fast Fourier transformation. Each FFT image was squared and subsequently averaged with other Fourier transformed frames. Since DNA images are isotropic, radial averaging of the Fourier image yields the radial structure factor $S(k)$ of the two-dimensional probe

$$S(k) = \langle\langle|\sum_{\mathbf{x}} I(\mathbf{x})\mathrm{e}^{i\mathbf{k}\cdot\mathbf{x}}|^2\rangle_{\text{frames}}\rangle_{\varphi} \qquad (6)$$

where φ denotes the radial averaging and $\mathbf{k}$ the lattice wave vector in units $2\pi/L$ with L being the width of the image. Note that averaging over different images of one sample corresponds to averaging the structure factor incoherently. Typically, $S(k)$ was averaged over 16 frames from three samples each. The coherence length of this artificial scattering experiment is naturally half the frame size. The structure factor was furthermore corrected with respect to the filter imposed by the optical transfer function, OTF(k), of the microscope.

$$\tilde{S}(k) = S(k)/|\mathrm{OTF}(k)|^2 \qquad (7)$$

The optical transfer function of the microscope setup was determined from a calibration image of 0.2 μm fluorescent latex beads fixed to a glass coverslip.

Results and Discussion

Conformation of Adsorbed DNA Chains. The shape of DNA chains is not expected to be an equilibrium conformation at the instant of adsorption from bulk solution onto a cationic membrane. We may consider the shapes of the molecules as random projections of a three-dimensional random coil onto two dimensions. Our observations confirm that the initial conformation of adsorbed chains is fairly globular. However, the chains expand during the early time course into visibly extended conformations. Relaxation occurs on a time scale of hours depending on bulk salt concentration. We interpret this early phase as disentanglement of a randomly adsorbed chain. The question arises whether, after some time, a meaningful equilibrium conformation is achieved. To this end we analyzed the distribution of fluorescence of individual chains in terms of moments according to eqs 1−3. In Figure 2 we showed examples of the time course of these moments. The quantity that shall interest us at this point is the extension of the chain as given by the second moment, the radius of gyration. Theory predicts power law behavior of the radius of gyration with chain length.

We produced fragments of λ-phage DNA (48.502 base pairs) using the restriction enzyme BbrPI. The λ-digest fragments consist of 880, 6141, 14 953, and 26 528 base pairs. A fluorescence image of the mixture adsorbed to a cationic membrane is given in Figure 3a. The three longer species are clearly visible, the shortest one is difficult to detect and was ignored in the analysis.

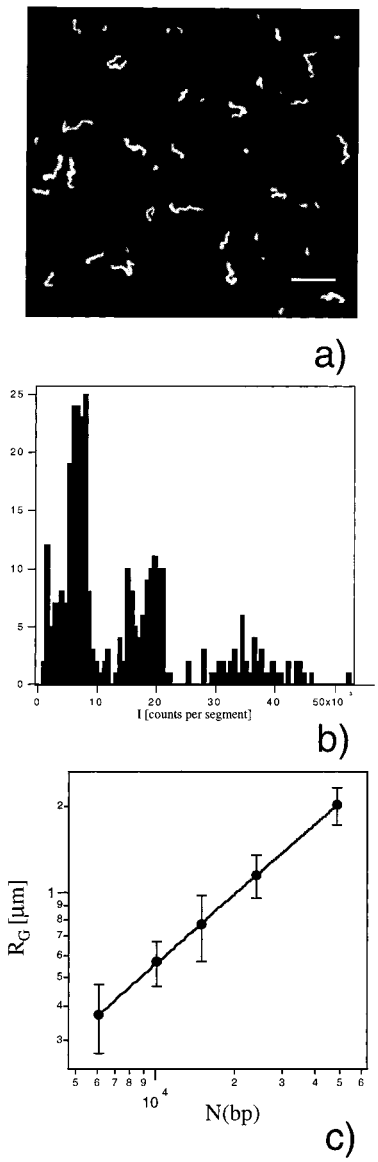

Figure 3. Static scaling analysis of single DNA molecules. (a) Fluorescence micrograph of λ-phage DNA cut by the restriction enzyme BbrPI. (b) Histogram of fragment fluorescence intensities. (c) The log−log plot of the averaged radius of gyration of λ-DNA fragments as a function of fragment length in number of base pairs N(bp). The straight line fits the scaling $R_G \propto N^{\nu}$ with $\nu = 0.79 \pm 0.04$.

A fluorescence intensity histogram of about 1000 molecules from 10 frames (Figure 3b) shows three maxima at intensities 8000 ± 2000, 17 000 ± 3000, and 37 000 ± 9000. Their relative ratio (1/2.1/4.6) is close to the ratio of the known length distribution of BbrPI fragments (1/1.8/4.3). This observation is equivalent to a classical restriction fragment length analysis.[17] The fact that the distribution is smeared out is due to inhomogeneous illumination, which is typically of flat Gaussian shape. However, this systematic variation is not interfering with the following analysis of single molecules, where only normalized moments of the distribution are considered.

We calculated the radius of gyration of about 300 individual molecules from λ digests of four different restriction enzymes. The averaged R_G values are plotted as a function of the number of base pairs (Figure 3c). In the log−log representation the radius of gyration scales

$$\langle R_G^2 \rangle \sim N^{2\nu} \tag{8}$$

with the number of base pairs, whereby the scaling exponents is found to be $\nu = 0.79 \pm 0.04$. This experimental value is in good agreement with the theoretical prediction $\nu = {}^3/_4$ for self-avoiding statistical chains in two dimensions. The exponent $\nu = {}^3/_4$ is known as the Flory−Edwards exponent, which in two dimensions turns out to be the exact exponent employing the self-consistent-field method[18,19] and renormalization theory.[20,21] The error bars in Figure 3c represent the numerical standard deviation of R_G, which is determined by the statistical properties of polymer chains. The mean-square deviation of the square of the radius of gyration

$$\frac{\langle (R_G^2 - \langle R_G^2 \rangle)^2 \rangle^{1/2}}{\langle R_G^2 \rangle} = \Delta R_G^2 \tag{9}$$

can be experimentally determined. We find $\Delta R_G^2 = 0.46$, which is somewhat smaller than the expected value for the ideal chain $\Delta R_G^2 = 0.5$. Chain fluctuations close to the ideal random walk value were also found in Monte Carlo simulations.[14]

From the experimental point of view we have to worry that the polymer shape is smeared out by the finite optical resolution of the microscope (in contrast to the zeroth and first moment, which are not affected by the optical resolution). However, numerical estimates assuming a Gaussian mass distribution of the molecule showed a negligible effect on the second moment of the fluorescence distribution for $R_G > 0.4$ μm. For this reason the shortest fragments investigated here were 6140 base pairs long.

Excluded-Volume Effect. Aside from the scaling behavior, also the absolute extension of the DNA chain can be investigated. From Figure 3c we find $R_G = 2.0$ μm for λ-phage DNA. In a self-consistent mean-field approach the radius of gyration of an excluded-volume polymer in two-dimensions is[18,19]

$$R_G = \left(\frac{a_F b_K^2}{12\pi}\right)^{1/4} N^{3/4} \tag{10}$$

which is equivalent to Florys result. Here b_K denotes the Kuhn length of a statistical independent chain segment and a_F the excluded volume, which in two dimensions we refer to as excluded area. The Kuhn length is known from experimental measurements of the persistence length $b_K = 2\xi_P \approx 0.1$ μm.[27] Hence, using eq 10 with $R_G = 2.0$ μm and $N = L/b_K = 170$, we obtain $a_F = 0.013$ μm^2. Theoretically, the excluded area parameter is defined as second virial coefficient by

$$a_F = \int_0^\infty (1 - e^{-w_{12}/kT})\, d^2r \tag{11}$$

where w_{12} denotes the interaction energy between two segments. Hence, we should be able to derive the excluded area parameter, if we know the dominating interaction between DNA segments.

The most obvious interaction between DNA segments is electrostatic repulsion. However, electrostatic interaction is not sufficient to explain the observed strongly swollen chain conformation. At a typical bulk salt concentration $c_{NaCl} = 10$ mM ($\kappa^{-1} = 3$ nm) the characteristic distance between two segments of the chain is much larger compared to the screening length $\sqrt{a_F} \gg 1/\kappa$. More importantly, experiment shows that the radius of gyration is not dependent on the bulk salt concentration in contrast to electrostatic models.

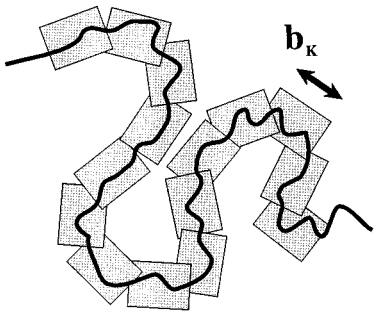

Figure 4. Schematic drawing of a self-avoiding semiflexible chain with overlay of hypothetical string of satistically independent segments of length b_K. The exluded area is of size b_K^2.

In the following we will argue that the self-avoidance constraint in two dimensions leads to a significant steric interaction, which is in agreement with the observed chain dimension. Consider the polymer chain divided into parts of length b_K as shown in Figure 4. Two segments are forbidden two cross each other in plane. For simplicity, we discuss the two limiting cases of two separated rods which are oriented either parallel or perpendicular to each other. For perpendicular segments the forbidden area is clearly $a_F = b_K^2$. Parallel rods are more complicated since they can approach each other but at the same time restrict their bending fluctuations. The free energy of confinement is $F = b_K kT/(d^{2/3} b_K^{1/3})$,[22,23] where d denotes the distance between the two segments. Hence, the excluded area is estimated calculating the distance d_c for which $F \approx k_B T$, yielding again $a_F = b_K^2$. Using this simplified argument for the excluded area in eq 10 and using the experimental Kuhn length $b_K = 0.1$ μm, we obtain an expected radius of gyration $R_G = 1.9$ μm, in good agreement with experiment. Note that the radius of gyration is no longer dependent on an specific interaction parameters but solely depends on the Kuhn length or likewise the persistence length. Under our conditions the latter is dominated by its elastic bending moduls which can be assumed to be identical in three dimensions and on surfaces. It is noteworthy that the described effect is due to the constraint of self-avoidance in reduced dimensionality. An analogy exists to fluctuating membranes in three dimensions, which likewise are impenetrable and give rise to the Helfrich steric interaction.[24]

Self-Diffusion and Rotational Relaxation of Single DNA Molecules. Adsorbed to fluid lipid membranes the DNA chains are confined to two dimensions but free to diffuse laterally. In the following we describe chain dynamics, self-diffusion of the molecules, and conformational relaxation. The overall motion of a single chain, i.e., the motion of center of mass, $\mathbf{R}_{cm}$, is described by its mean-square displacement

$$\langle |\mathbf{R}_{cm}(t) - \mathbf{R}_{cm}(0)|^2 \rangle = 4Dt \tag{12}$$

Examples of mean-square displacement versus time plots are given in Figure 5a for 6 and 10 kbp DNA. Self-diffusion coefficients of 2−5 chain trajectories were determined and averaged separately for DNA-restriction fragments ranging from 1 to 49 kbp in length. In the course of the analysis it appeared that several trajec-

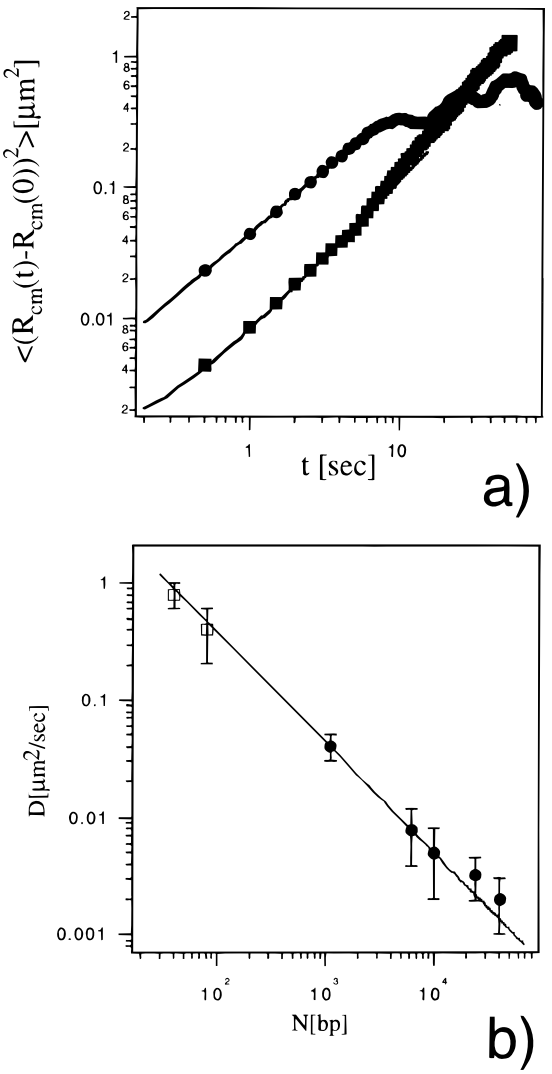

Figure 5. DNA self-diffusion. (a) Double-logarithmic plot of the mean-square displacement of center of mass versus time shown for two fragments with 10 kbp (■) and 6 kbp (●). (b) Scaling behavior of the self-diffusion coefficients derived from (a). Straight line indicates slope −1. The data points for 40 and 80 bp oligonucleotides (open squares) were obtained from fluorescence recovery after photobleaching measurements.[26]

tories exhibited anomalous diffusion. This phenomenon is attributed to surface defects that impose invisible diffusion barriers to DNA as discussed in the last section of this article. For the present analysis the few molecules with anomalous diffusion were discarded in order to prevent biased scaling behavior. Furthermore, two populations of very short fragments (40 and 80 bp) were investigated using fluorescence recovery after photobleaching.[28] The resulting power law dependence of the diffusion coefficient D_{cm} as a function of restriction fragment size is shown in a log−log presentation (Figure 5b). The best fit to the experimental data yields $D_{cm} \propto N^{-0.95\pm0.06}$. Hence, the self-diffusion decreases inversely proportional to the length of the polymer as predicted for the dynamical scaling of the Rouse model, $D_{Rouse} \propto N^{-1}$, in the absence of hydrodynamic interaction. This finding is substantially different from DNA three-dimensional self-diffusion in bulk, where long-ranged hydrodynamic interaction plays a dominant role. In fact, comparable DNA experiments[3] in bulk water showed Zimm dynamics, $D_{Zimm} \propto N^{-3/5}$. At the membrane surface, however, the hydrodynamic interaction is screened due to the strong frictional coupling between polymer and membrane. Theoretically this situation has been considered for polymers embedded in a fluid membrane.[26,27]

The observed polymer shapes appear to be highly asymmetric. According to theoretical studies, an instantaneous polymer configuration may rather be described by an ellipse than a centrosymmetric plate.[16,28] Thus, the simplest conformational change is the rotational motion of an ellipse.[2,30] Figure 6a shows a time sequence of a single molecule with overlay of the unit vector $\mathbf{u}(t)$ defined as the direction of the longer principal axis of the gyration tensor. The time correlation function of $\mathbf{u}(t)$ decays exponentially

$$\langle \mathbf{u}(t)\ \mathbf{u}(0)\rangle \propto \exp\left(-\frac{t}{\tau_r}\right) \tag{13}$$

where τ_r denotes the rotational relaxation time (Figure 6b). As shown in Figure 6c, the rotational relaxation time varies as a power of length, $\tau_r \propto N^{\mu}$ with $\mu = 2.6 \pm 0.4$. Using the idea of dynamical scaling, the scaling behavior of the rotational relaxation follows from the Rouse model and the Flory exponent ν.

$$\tau_r \propto N^{1+2\nu} \tag{14}$$

Inserting the Flory exponent $\nu = {}^3/_4$, we obtain $\mu_{theory} = 2.5$, in remarkable agreement with the experimental result.

Structure Factor of Dilute Two-Dimensional DNA Solutions. In the following two sections we will no longer analyze individual molecules but rather demonstrate that ensembles of adsorbed DNA strands exhibit well-behaved collective polymer properties on a cationic supported membrane. Figure 7a shows a fluorescence micrograph of λ-DNA, which represents a real space image of a monodisperse two-dimensional polymer solution. The quantity of interest is the structure factor, which in this case can be calculated by Fourier transformation of the entire image. Figure 7b depicts the absolute value of the Fourier transform, which is centrosymmetric and hence readily circularly averaged and plotted versus the wave vector $k_n = n \cdot 2\pi/L$. In Figure 7c a Zimm plot of the structure factor is given, which allows to extract the radius of gyration R_G of λ-DNA from the small k-vector region according to

$$S^{-1}(k) = S^{-1}(k \to 0)\left(1 + \frac{k^2 R_G^2}{2}\right) \tag{15}$$

Note that the factor ${}^1/_2$ indicates the spatial dimension $d = 2$. As should be expected, the Zimm plot (Figure 7c) yields $R_G = 1.7 \pm 0.3\ \mu$m, in agreement with the value derived from the moment analysis in real space.

In an intermediary wave vector regime regime $1/R_G < k < 1/b_K$ the structure factor follows a power law

$$S(k) \propto k^{-1/\nu} \tag{16}$$

where the experimental slope is found to correspond to a fractal exponent $\nu = 0.71$. The scaling indicates the self-similar structure of an excluded-volume polymer ($\nu = {}^3/_4$). In Figure 7d the upper limit for this scaling regime is determined by the optical resolution $2\pi/l_{opt}$ (dashed line) rather than the Kuhn length of the polymer.

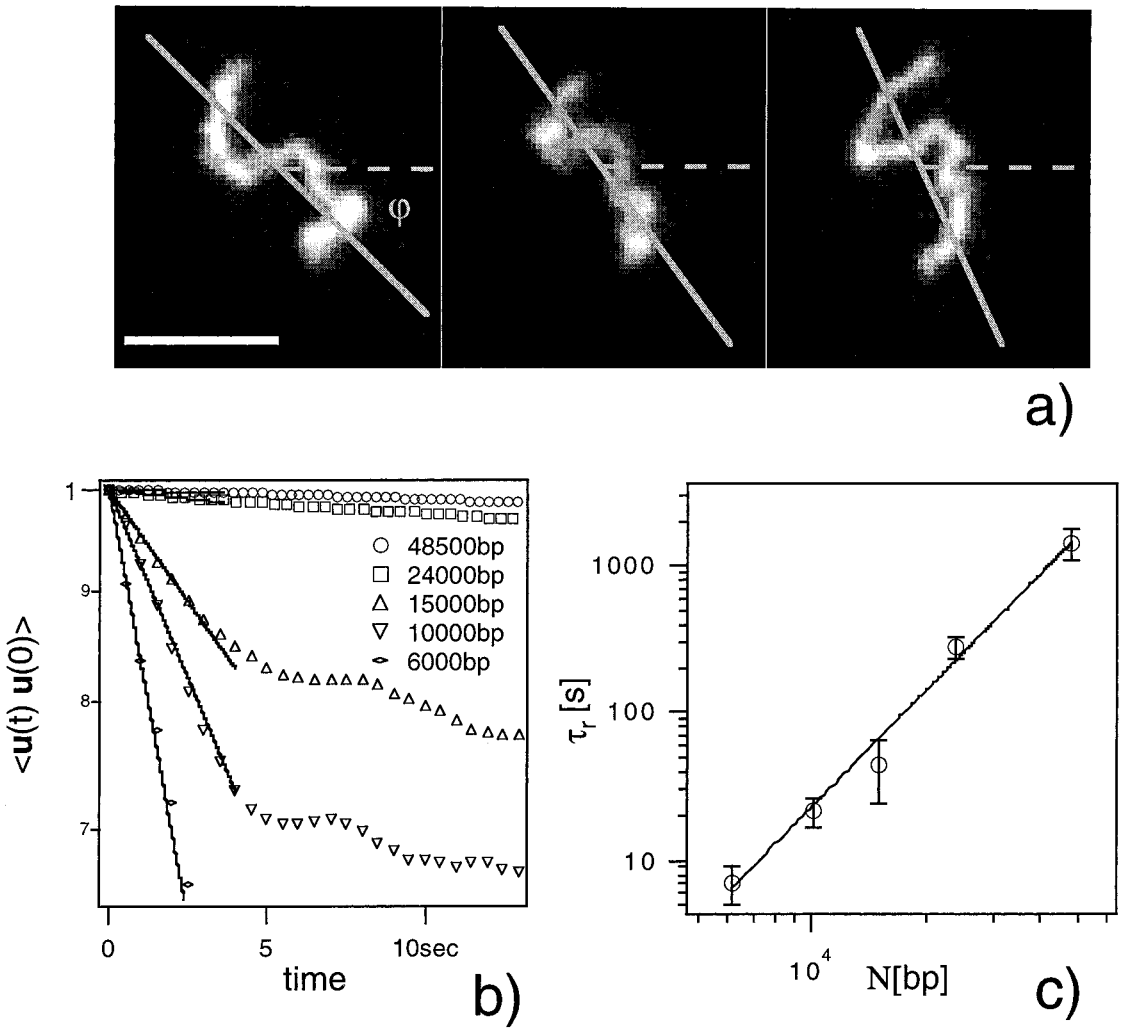

Figure 6. Rotational relaxation of single DNA molecules. (a) Time sequence of a single DNA molecule with overlay of the longer principal axis of the gyration tensor. (b) The angle φ of the corresponding unit vector varies in time due to Brownian motion of the molecule. The computational analysis of the gyration tensor shows discontinuities by $\pi/2$ (arrow), if major and minor axis interchange as described in the text. (c) The time correlation function of the unit vector decays such as a single exponential with rotational relaxation time τ_r. (d) The rotational relaxation shows scaling behavior $\tau_r \propto N^{2.6\pm0.4}$.

In this context we would like to address some pitfalls of the seemingly straightforward data analysis. Fluorescently labeled DNA is usually subject to photodamage as can be seen for example in the presence of small fragments in Figure 7a. However, in our case polydispersity affects the Zimm plot analysis of R_G to a negligible degree. Even if 20 mol % DNA molecules is assumed fractured, we estimate a systematic deviation of R_G toward smaller values of order 10% using the expressions for polydispersity in ref 29. Naturally the fractal scaling is not affected by polydispersity, but great care has to be taken in the optical image correction. Background noise, we found, is flat in the intermediate length scale regime but adds a constant offset to the scattering function. More importantly, the optical transfer function corrects the data significantly in the scaling regime. Hence, it turned out to be crucial to use an experimental transfer function obtained from submicron fluorescent latex beads.

For all practical purposes, the determination of R_G and the determination of the static scaling exponent are more reliably done by direct analysis in real space. However, as soon as we move toward more concentrated DNA layers, the Fourier analysis yields additional information.

Semidilute Solutions in Two Dimensions. As the surface coverage exceeds the concentration $c^* = 1/\pi R_G^2$, the chains start to overlap each other. For λ-DNA the crossover concentration is $c^* \approx 0.07\ \mu m^{-2}$. In an attempt to produce semidilute polymer solutions, we incubated increased concentrations of λ-DNA onto a cationic supported membrane. The incubation was stopped after 5 min by thorough rinsing with DNA-free solution. The system then was left to equilibrate over a period of 2 days. Figure 8a−c shows images of the resulting semidilute solution. The snapshots are taken at the same sample position in 30 min time intervals. The distribution of chains is dynamic as can be seen by the evolution of the apparent holes in the surface coverage indicated in Figure 8a. The holes disappear and seem to arise elsewhere on the surface (Figure 8b,c). Averaged over a long period of time, however, the surface coverage is homogeneous. Its is reasonable to assume a Zernike−Ornstein type structure factor for the semidilute regime.[30,31]

$$S(k) \propto \frac{1}{1 + k^2\xi^2} \tag{17}$$

where ξ denotes the correlation length. In the following we consider directly the pair-correlation function of the

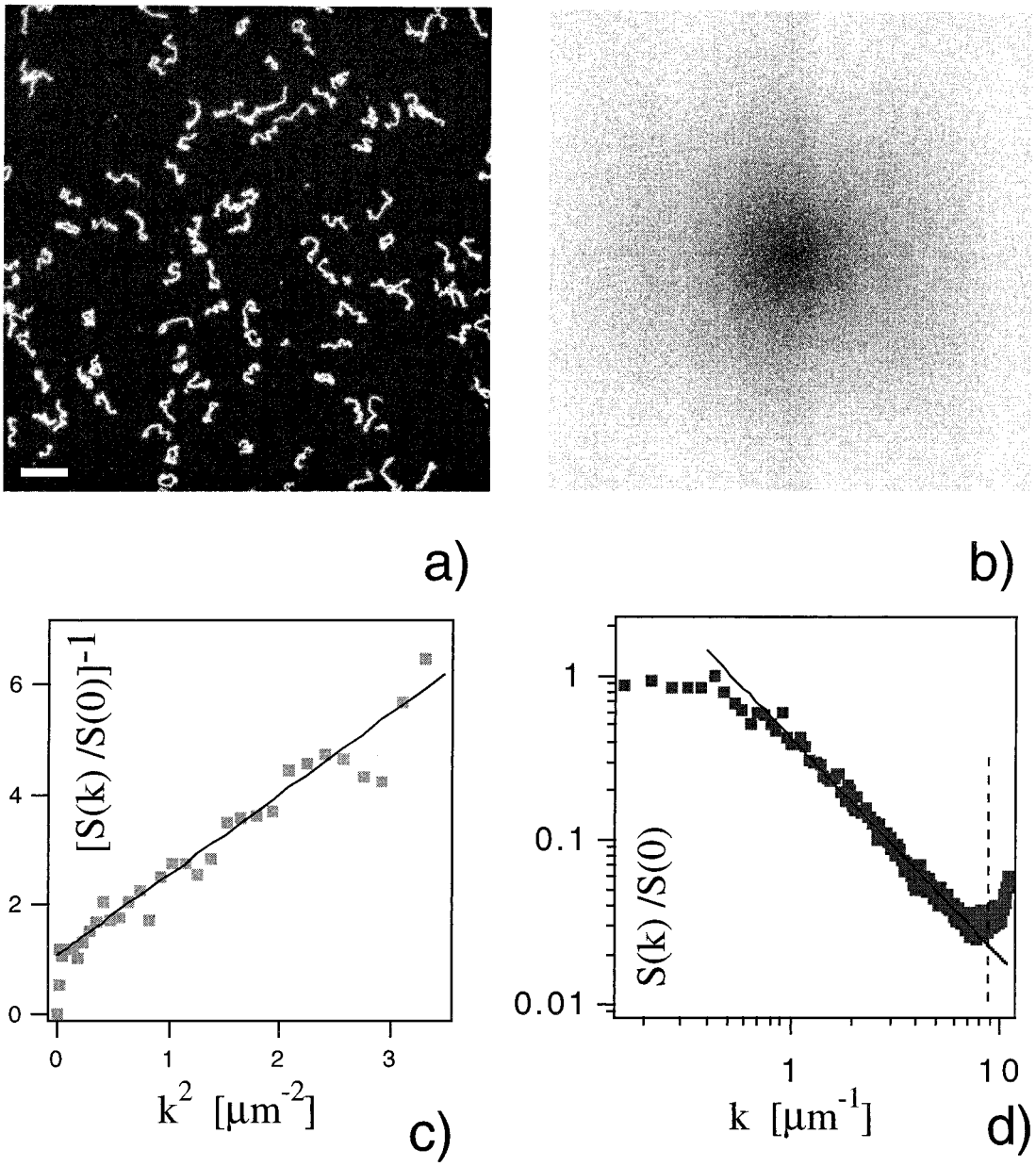

Figure 7. Polymer properties of dilute 2D DNA solutions. (a) Micrograph of monodisperse λ-DNA on a cationic lipid membrane. (b) Fourier transformed image of (a). (c) Structure factor derived from (b) plotted versus radial wave vector $k = 2\pi/r$ squared (Zimm plot). The small angle regime yields $R_G = 1.7 \pm 0.3\ \mu$m. (For the fit the first three modes are not taken into account since they result from heterogeneous illumination of the sample.) (d) The log−log plot of the structure factor $S(k)$ exhibits fractal scaling $S(k) \propto k^{-1/\nu}$ in the region $2\pi/R_G \ll k \ll 2\pi/l_{opt}$, where l_{opt} denotes the optical resolution limit of the microscope (dashed line). The straight line exhibits slope -1.4 ± 0.1.

polymer solution, which is obtained by two-dimensional Fourier transformation of $S(k)$.

$$\langle I(r)\, I(0)\rangle \propto F^{-1}(S(k)) \propto \int_0^\infty \frac{1}{1+k^2\xi^2} J_0(kr)k\, \mathrm{d}k \propto K_0\left(\frac{r}{\xi}\right) \quad (18)$$

The leading terms of the Bessel function K_0 are

$$\langle I(r)\, I(0)\rangle \propto \sqrt{\frac{\xi}{r}} \exp\left(-\frac{r}{\xi}\right)\left[1 + O\left(\frac{\xi}{r}\right)\right] \quad (19)$$

Figure 8d presents the experimental correlation function with best fits using eq 19. The data yield an apparent correlation length $\xi = 1.3 \pm 0.4\ \mu$m. For comparison, the correlation function of the dilute solution as discussed in Figure 7 is plotted on top. The dilute curve decays with apparent correlation length $\xi = 1.7 \pm 0.4\ \mu$m, in agreement with the radius of gyration $\xi = R_G/\sqrt{2}$. The correlation length of the semidilute regime is shorter than in the dilute case as expected.[30,31] Note that the experimental correlation functions approach asymptotically to zero. This was achieved by cutting out the average fluorescence intensity S(k=0) and also the illumination skewness $S(k=2\pi/L)$ prior to the Fourier back-transformation. To achieve data with proper asymptotic behavior, it is essential that the DNA solution is homogeneously prepared and well equilibrated. At high surface coverage this is difficult to achieve, and artificial long-ranged correlations are frequently seen.

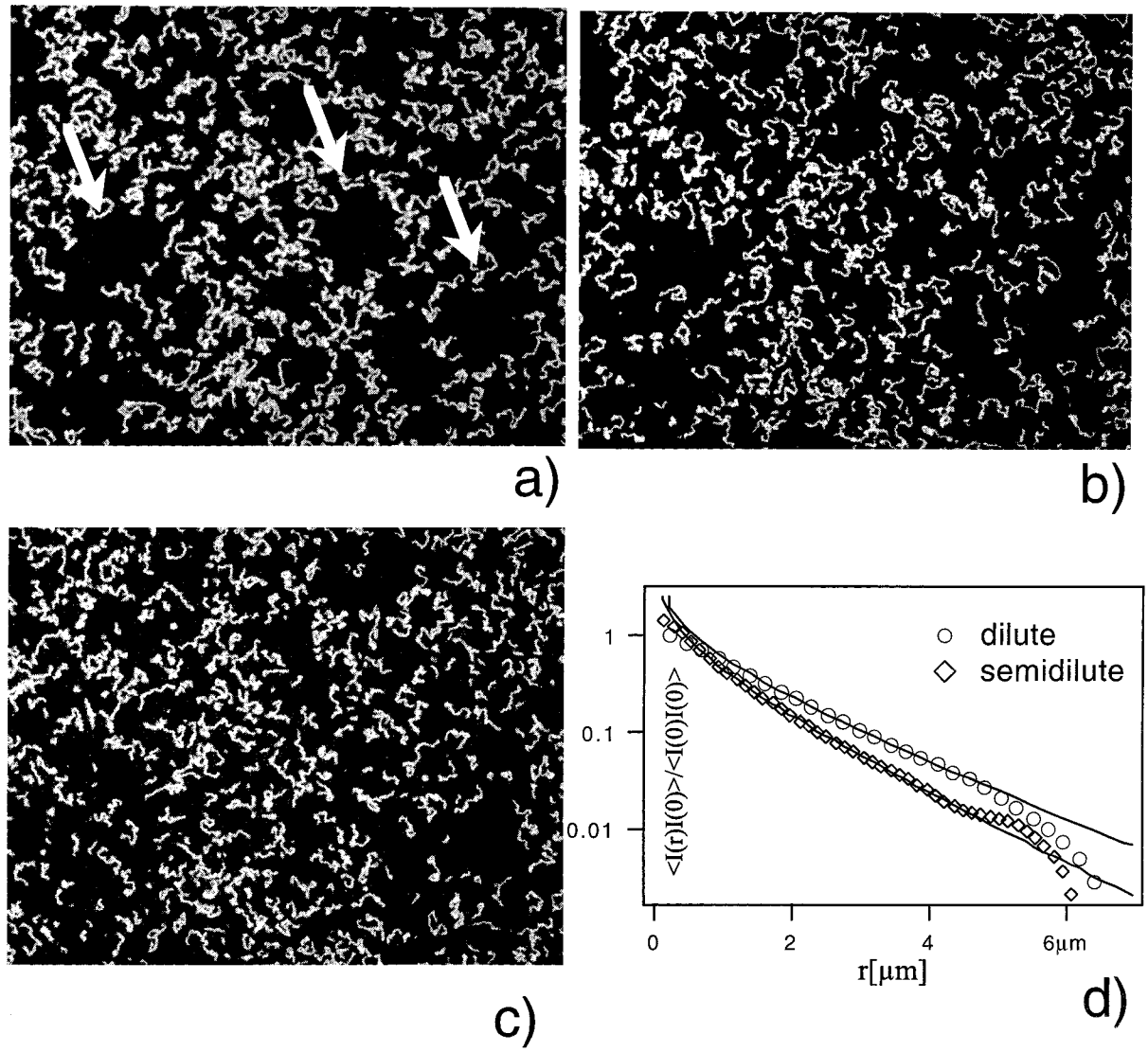

Figure 8. Semidilute solution of λ-DNA confined to a lipid membrane in 10 mM HEPES, 30 mM NaCl, 0.5 mM ascorbic acid, pH 7. (a−c) Micrographs taken in 30 min time intervals. The arrows indicate dynamic density fluctuations (apparent holes), which disappear over a periode of 1 h. (d) Intensity autocorrelation function of the semidilute preparation shown in (a−c) and dilute solutions (Figure 4). The fit yields correlation lengths $\xi = 1.7 \pm 0.4$ for dilute and $\xi = 1.3 \pm 0.4$ for the semidilute solution.

Unbinding of DNA from Cationic Membranes. The bulk salt concentration screens the electrostatic interaction between DNA segments as well as between DNA and the oppositely charged membrane. We find that DNA on a 10% charged membrane (DOPC/DOTAP, 10:1) desorbs at salt concentrations larger than 50 mM (Figure 9a). Theoretically, the adsorption of semiflexible polyelectrolytes from an oppositely charged surface was treated by Netz and Joanny.[22] It turns out that on a low dielectric surface (like a hydrocarbon lipid membrane), a stable minimum between the electrostatic Debye−Hückel attraction and image-charge repulsion exists. In this case the vertical width of a layer of semiflexible polymers is of order $\delta \sim \tau/\sigma$, where τ is the polymer line charge density and σ the surface charge density. Unbinding occurs, if the width δ exceeds the Debye screening length $\delta \geq \kappa^{-1} \approx 2$ nm at 50 mM salt concentration. We estimate the surface charge density $\sigma = 0.25$ nm^{-2} from the molar ratio of charged and uncharged lipids. Thus, we yield an effective line charge density $\tau = {}^1/_2$ nm^{-1} about a factor of 2 below the inverse Bjerrum length expected for Manning condensation of counterions from the buffer solution. This discrepancy most probably results from the helical arrangement of the charges along the DNA backbone which is poorly described by an infinetely thin rod as assumed in the theory.

In the absence of bulk salt the cationic lipids are believed to play the role of two-dimensional counterions.[32] In Figure 9b,c we show that negatively charged fluorescently labeled lipids are displaced from the location of the DNA strand. In contrast, at 10 mM salt concentration the underlying lipid membrane is entirely homogeneous. Similar demixing at low ionic strength has been observed for basic peptides bound to acidic lipid membranes.[33]

Diffusion around Obstacles. Defects are a common problem in surface studies. Surface defects may be dust particles on the membrane surface, which remain invisible in light microscopy but affect the diffusion of DNA. It is important to be aware of potential impediment by defects. Two kinds of phenomena were observed: First, DNA is pinned, and hence the self-diffusion of the center of mass is confined for long time scales. In this case the mean-square displacement follows anomalous diffusion $\langle |R_{cm}(t) - R_{cm}(0)|^2 \rangle \propto t^{\alpha}$ with $\alpha < 1$. The second kind of

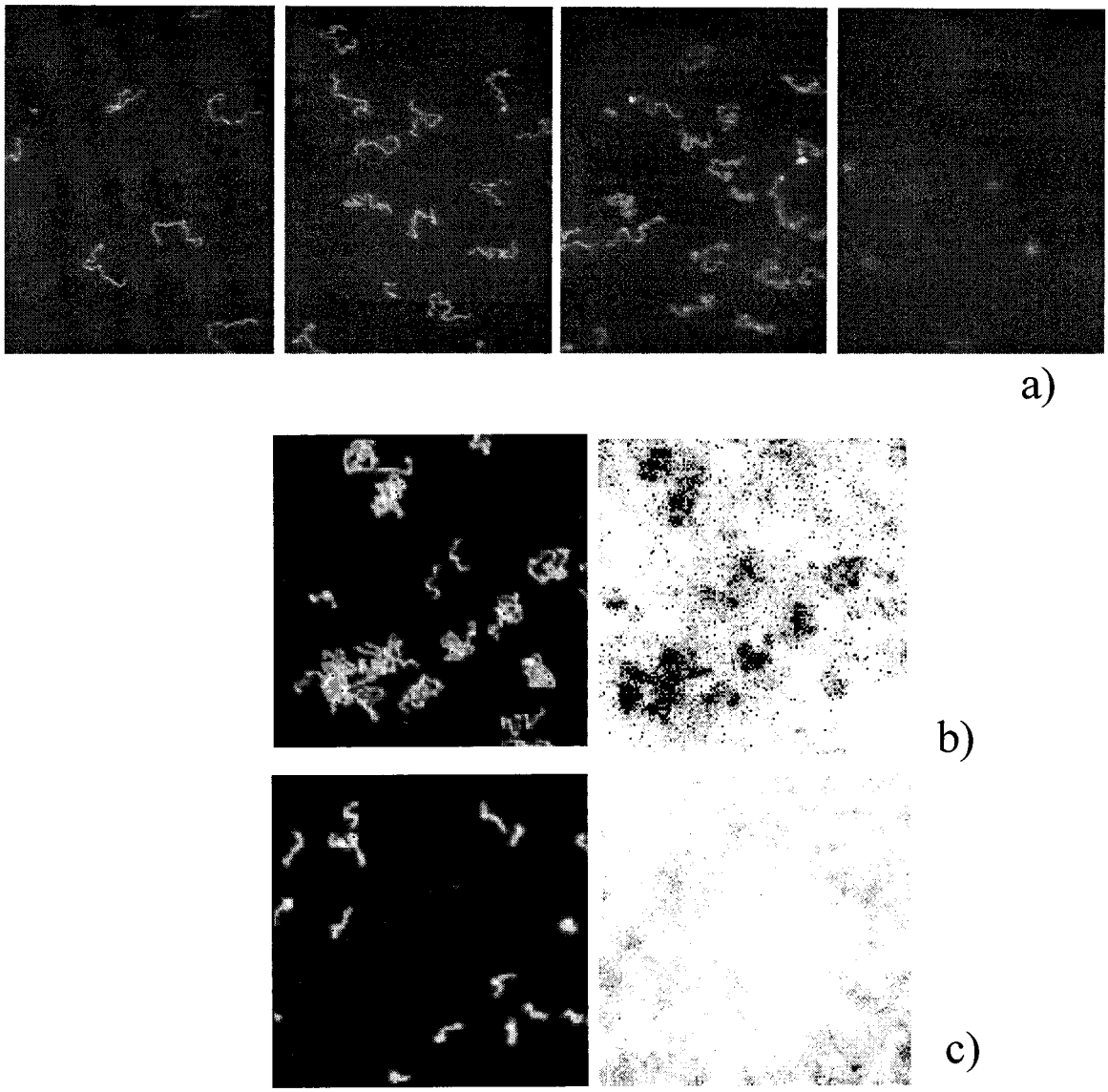

Figure 9. DNA-desorption. (a) Unbinding of DNA from a 10% charged membrane (DOPC/DOTAP 10:1) in 10 mM HEPES, pH 7, buffer with increasing salt concentration from left to right (10, 20, 30, and 50 mM NaCl). (b) Comparison of the DNA fluorescence (left) and lipid fluorescence (right) distribution. At low ionic strength DNA induces local demixing of the lipid membrane. (c) In 10 mM HEPES, pH 7, the membrane fluorescence becomes homogeneous.

behavior is the encounter of diffusion barriers. When analyzing the motion of single molecules by animation of sequences of micrographs, obstacles show up as invisible diffusion barriers.

Conclusion

Is DNA on cationic lipid membranes useful as a model system in polymer science? We have shown in this article that the polymer behavior of single chains is well described by classical polymer physics of self-avoiding walks in two dimensions. Moreover, we demonstrated that crowded surfaces exhibit the predicted collective properties. The agreement with theory is indeed encouraging and opens the way to more sophisticated experiments on this basis. Three facts are remarkable about DNA on cationic membranes. First, the persistence length is just below the optical resolution, which lets the polymer appear flexible on the microscopic length scale. Second, as shown in this article, the monomer−monomer interaction is repulsive, and the model polymer is in good solvent conditions. Finally, DNA is semiflexible on a molecular scale which leads to the fact that the chain is bound flat to the oppositely charged membrane over a wide regime of ionic strength. Surface bound DNA has the technical advantage that no out-of-plane corrections need to be considered. Direct imaging of single polymers is able to address the question of polymer shapes which is difficult to access otherwise. An example is the rotational relaxation examined here. Furthermore, experiments are in progress that will address the structure of polymer solutions in the semidilute and concentrated regime in more detail. We showed that meaningful correlation length can be derived by Fourier analysis of equilibrated samples. Theoretical predictions for the density scaling[34] and as well as the dynamics exist.[38] A dimensional speciality is also the fact that in two dimensions self-avoiding chains cannot entangle, and for DNA on cationic membranes chains have been seen to segregate at higher concentrations.[12] In this context an additional technical feature is the possibility to mix two populations of DNA labeled with two different colors. Two-color labeling would allow to separate intramolecular and intermolecular correlations equivalent to deuteration in neutron

experiments. The presence of obstacles is a major problem for dynamical measurements on long time scales. Similarly, obstacles are seen in lipid membrane spreading experiments.[35] Since most random obstacles are dust related, special care has to be taken in sample preparation. On the other hand, engineered obstacles bear interesting prospect to micromanipulate DNA on cationic membranes for biotechnological purposes. Silicon devices with grids of micron-size posts in a quasi-two-dimensional flow channel are used to separate DNA.[9] Similarly, microstructured membrane-coated surface are amendable for separation purposes.[36] Thus, cationic lipid membranes could be useful as well-controlled fluid binding surface for DNA.

Acknowledgment. We thank Prof. Sackmann for his interest in this work and support through resources available at the Biophysics Institute. We also enjoyed fruitful discussion with Mathias Fuchs and Roland Netz. This work was funded by the Deutsche Forschungs-Gemeinschaft through Grant SFB266-C14.

References and Notes

(1) For review see: Bustamante, C. *Annu. Rev. Biophys. Biophys. Chem.* **1991**, *20*, 415−446.
(2) Matsumoto, M.; Sakaguchi, T.; Kimura, H.; Minagawa, K.; Matsuzawa, Y.; Yoshikawa, Y.; Doi, M. *J. Polym. Sci., Part. B* **1992**, *30*, 779−783.
(3) Smith, D. E.; Perkins, T. T.; Chu, S. *Macromolecules* **1996**, *29*, 1372−1373.
(4) Perkins, T. T.; Smith, D. E.; Larson, R. G.; Chu, S. *Science* **1995**, *268*, 83−87.
(5) Manneville, S.; Cluzel, P.; Viovy, J.-L.; Chatenay, D.; Caron, F. *Eur. Phys. Lett.* **1996**, *36*, 413−418.
(6) Käs, J.; Strey, H.; Sackmann, E. *Nature* **1994**, *368*, 226−229.
(7) Perkins, T. T.; Douglas, E. S.; Chu, S. *Science* **1994**, *264*, 819−822.
(8) Smith, S. B.; Aldridge, P. K.; Callis, J. B. *Science* **1989**, *243*, 203−206.
(9) Bakajin, O. B.; Duke, T. A. J.; Chou, C. F.; Chan, S. S.; Austin, R. H.; Cox, E. C. *Phys. Rev. Lett.* **1998**, *80*, 2737−2740.
(10) Mel'nikov, S. M.; Sergeyev, V. G.; Yoshikawa, K. *J. Am. Chem. Soc.* **1995**, *117*, 2401.
(11) Brewer, L. R.; Corzett, M. Balhorn, R. *Science* **1999**, *286*, 120−123.
(12) Maier, B.; Rädler, J. O. *Phys. Rev. Lett.* **1999**, *82*, 1911−1914.
(13) Cloizeaux, J.; Jannink, G. *Polymers in Solution*; Clarendon Press: Oxford, 1990.
(14) Carmesin, I.; Kremer, K. *J. Phys. (Paris)* **1990**, *51*, 915−932.
(15) Milchev, A.; Binder, K. *Macromolecules* **1996**, *29*, 343−354.
(16) Doi, M.; Nakajima, H. *J. Chem. Phys.* **1974**, *6*, 124−129.
(17) Schwarz, D. C.; Li, X.; Hernandez, L. I.; Ramnarain, S. P.; Huff, E. J.; Wang, Y.-K. *Science* **1993**, *262*, 110−114.
(18) Edwards, S. F. *Proc. Phys. Soc. London* **1965**, *85*, 613−624.
(19) Pereira, G. *J. Phys. A: Math. Gen.* **1997**, *30*, 467−483.
(20) Cardy, J. L.; Hamber, H. W. *Phys. Rev. Lett.* **1980**, *45*, 499.
(21) Nienhuis, B. *Phys. Rev. Lett.* **1982**, *49*, 1062.
(22) Netz, R.; Joanny, J.-F. *Macromolecules* **1999**, *32*, 9013−9025.
(23) Odijk, T. *Macromolecules* **1983**, *16*, 1340−1344.
(24) Sornette, D.; Ostrowsky, N. In *Micelles, Membranes, Microemulsions and Monolayers*; Gelbhart, W. M., Ben-Shaul, A., Roux, D., Eds.; Springer-Verlag: Berlin, 1994.
(25) Zantl, R.; Clausen-Schaumann, H.; Rädler, J. O., to be published.
(26) Muthukumar, M. *J. Chem. Phys* **1985**, *82*, 5696−5706.
(27) Komura, S.; Seki, K. *J. Phys. II* **1995**, *5*, 5−9.
(28) Aronovitz, J. A. Nelson, D. R. *J. Phys. (Paris)* **1986**, *47*, 1445−1456.
(29) Higgins, J. S.; Benoît, H. C. *Polymers and Neutron Scattering*; Oxford Science Publications: New York, 1994.
(30) Doi, M.; Edwards, S. F. *The Theory of Polymer Dynamics*; Clarendon Press: Oxford, UK, 1986.
(31) Fuchs, M.; Müller, M. *Phys. Rev. E* **1999**, *60*, 1921−1929.
(32) Bruinsma, R. Mashl, J. *Europhys. Lett.* **1998**, *41*, 165−170.
(33) Denisov, G.; Wanaski, S.; Luan, P.; Glaser, M McLaughlin, S. *Biophys. J.* **1998**, *74*, 731−744.
(34) Fuchs, M.; Schweizer, K. S. *J. Chem. Phys.* **1997**, *106*, 347−375.
(35) Nissen, J.; Gritsch, S.; Wiegand, G.; Rädler, J. O. *Eur. Phys. J. B* **1999**, *10*, 335−344.
(36) Van Oudenaarden, A.; Boxer, S. *Science* **1999**, *285*, 1046−1048.
(37) Hagerman, P. J. *Annu. Rev. Biophys. Biophys. Chem.* **1988**, *17*, 265−286.
(38) Herminghaus, S.; Hjelt, T.; Leiderer, P. *Phys. Rev. Lett.* **1996**, *76*, 4003−4006.

MA000075N